Lalit Prasad et al. International Journal of Recent Research Aspects ISSN: 2349-7688, Vol. 4, Issue 2, June 2017, pp. 47-52

Theoretical And Experimental Proof Of Mix-Valent Dinuclear Phenoxo-/Acetato-Bridged Manganese (II,III) Complex With Labile Sites

Lalit Prasad[1], Shafat Ahmad Khan[1], Himanshu Arora[2,3]

[1]Department of Chemistry, Galgotias University, Greater Noida, India
[2]Indian Institute of Technology Kanpur, India
[3]Department of Basic and Applied Science, GD Goenka University, Gurgaon, India

***Abstract*— Using the dinucleating phenol-based ligand 2,6-bis[3-(pyridin-2-yl)pyrazol-1-ylmethyl]-4-methyl phenol] (L^1OH), in its deprotonated form, the two dinuclear complexes $[Mn^{II}_2(\mu\text{-}OL^1)(\mu\text{-}O_2CMe)_2(CH_3CN)_2][PF_6]$ and $[Mn^{II}_2(\mu\text{-}OL^1)(\mu\text{-}O_2CMe)_2(CH_3CN)_2]$ $[BPh_4]$ have been chosen to study their electronic structure both experimentally as well theoretically. The physicochemical properties (absorption spectral data, 1a,b) of the cation of 1a is identical with that of 1b. In this work, we present a comprehensive report on the redox chemistry of $[Mn^{II}_2(\mu\text{-}OL^1)(\mu\text{-}O_2CMe)_2(CH_3CN)_2][PF_6]$ (1a). To throw light on the site of oxidation (metal or ligand-centered) in 1a, Density Functional Theory (DFT) calculations have been performed on $[Mn^{II}_2(\mu\text{-}OL^1)(\mu\text{-}O_2CMe)_2(CH_3CN)_2][BPh_4]\cdot 2CH_3CN$ (1b) at the B3LYP level of theory. Cyclic voltammetric experiments show a quasi-reversible process at $E_{1/2}$ = 0.70 V vs SCE. Coulometric oxidation in dry CH_3CN produced the one-electron oxidized product $Mn^{III}Mn^{II}$, which is found to be unstable towards reduction. We assign the electronic structure of $Mn^{II}Mn^{II}$ dimer and its one-electron oxidized product $Mn^{III}Mn^{II}$ through DFT calculations. During one-electron oxidation of 1b only one Mn atom is losing electron and other one is redox innocent. DFT calculations indicate that the redox process has significant ligand character. Increase in the oxidation state of Mn^{II} results in enhanced charge donation from ligand to metal ion.**

***Keywords*—** *Phenoxo-bridged complex, redox property, mix-valent species, density functional theory*

I. INTRODUCTION

Bimetallic cores exist at active sites of many enzymes and play an essential role in biological systems. The present work derives impetus from the active sites of metalloproteins.[1-3] The bridge functions to maintain the two metal centers in close proximity under conditions where simple oxo-bridged complexes are known to dissociate.[2,4] Dinuclear manganese complexes constitute the active sites of several redox enzymes such as manganese catalases,[5] and hydrolytic enzymes such as arginase,[5] among others.[5] The manganese ions are often found to be bridged by at least one carboxylate (from glutamate or aspartate) and water, hydroxide ion or oxide. Among the manganese catalases and model complexes of dinuclear Mn^{II} active sites, weak antiferromagnetic interactions are observed between the bridged metal ions.[6] Our main concern of this investigation is to study the electronic structure of the complex.

A dinucleating ligand such as L^1OH (Scheme 1) which provide a phenoxo oxygen for the endogenous bridging of the two metal ions and the two arms with bidentate donor sets is expected to maintain the integrity of the dinuclear center in the solid as well as in solution, through change in the metal oxidation states.[7] In addition, m-xylyl ring in L^1O^- connecting the chelating arms provides a rigid spacer for a bridged dinuclear complex. This confers an entropic advantage in concerted reactions of two metal ions.[8] From this perspective, we describe herein μ-phenoxo-bis(μ-carboxylato)-bridged complex of Mn^{II} ion of L^1O^-, comprising of one phenolate group and two pyridylpyrazole units. Specifically, we present a comprehensive report on the redox chemistry of $[Mn^{II}_2(\mu\text{-}OL^1)(\mu\text{-}OAc)_2(CH_3CN)_2][PF_6]$ (**1a**). To throw light on the site of oxidation (metal or ligand-centered) in **1a**, Density Functional Theory (DFT) calculations have been performed on $[Mn^{II}_2(\mu\text{-}OL^1)(\mu\text{-}OAc)_2(CH_3CN)_2][BPh_4]\cdot 2CH_3CN$ (**1b**) at the B3LYP level of theory.

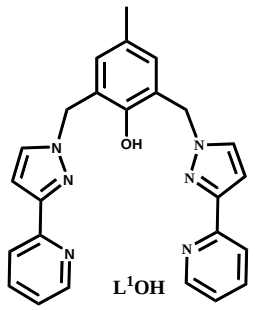

L^1OH

Scheme 1

In this work an attempt has been made to do the DFT calculations on the parent compound **1b** as well as on its one-electron oxidized species to understand the electronic structure of the latter species. It is worth mentioning here that in recent years DFT is commonly used to examine the electronic structure of transition metal complexes. It meets with the requirements of being accurate, easy to use, and fast enough to allow the study of relatively large molecules of transition metal complexes.[9]

II. MATERIAL AND METHODS

General Procedure. All reagents and solvents were obtained from commercial sources and used as received. Solvents were

dried/purified as reported previously.[10] The synthesis of 3-(2-pyridyl)pyrazole was achieved following a reported procedure.[11] The ligand L^1OH and $[Mn^{II}_2(\mu\text{-}OL^1)(\mu\text{-}OAc)_2(CH_3CN)_2][PF_6]$ (**1a**) and $[Mn^{II}_2(\mu\text{-}OL^1)(\mu\text{-}OAc)_2(CH_3CN)_2][BPh_4]$ (**1b**) were synthesized as before.[10]

Physical Measurements. Spectroscopic measurements were made using the following instruments: Bruker Vector 22; electronic, Perkin Elmer Lambda 2 and Agilent 8453 diode-array spectrophotometer; X-band EPR, Varian 109 C (fitted with a quartz dewar for measurements at liquid-dinitrogen temperature), the spectra were calibrated with diphenylpicrylhydrazyl, DPPH (g = 2.0037). Cyclic voltammetric experiments were performed at 298 K by using a PAR model 370 electrochemistry system consisting of M-174A polarographic analyzer, M-175 universal programmer, and RE 0074 X-Y recorder. The cell contained a Beckman (M 39273) platinum-inlay working electrode, a Pt wire auxiliary electrode, and a saturated calomel electrode (SCE) as reference electrode. Details of the cell configuration are as described before.[12] For coulometry a platinum-wire-gauze was used as the working electrode. The solutions were ~ 1.0 mM in complex and 0.1 M in supporting electrolyte, TBAP.

Theoretical Studies. DFT calculations have been performed using the Gaussian 03 program.[13] Optimized molecular geometries were calculated using the B3LYP exchange-correlation functional.[14] The spin-unrestricted DFT method was employed to model these open-shell species. Geometry optimization has been done for both the reduced and oxidized species. All the atoms were described using the 3-21G basis sets. Wave function stability calculations were performed to confirm that the calculated wave functions corresponded to the ground state. Single-point and NBO calculations were performed on the optimized structures of the complexes for molecular orbital analysis. Atomic charges and spin densities were calculated using Mulliken[15] and natural[16] population analysis (MPA and NPA, respectively) as implemented in Gaussian 03.

III. Results and Discussion

The absorption spectral property of **1a** is identical with those of **1b**, which suggests that the core structure remains invariant in the two sets of complexes with PF_6^-/BPh_4^- anions.[10] Reactivity studies were done with PF_6^- salts, due to solubility reasons. A perspective view of the cationic part of the complex 1b, with atom-labeling scheme is shown in Fig. 1.

EPR Spectra. Dinuclear manganese complexes give characteristic X-band EPR spectra depending on metal oxidation states, ligation environment, and the nature of the bridging ligands, which determines the degree of exchange coupling between the metal ions. One expects 11 lines from a Mn^{II} dimer on the basis of the equation 2(2)I + 1 at lower temperature below 40 K.[17] In our system, we observed only six hyperfine structure with g centered around 1.99. It is because of the fact that at 120 K, the other hyperfine structures are not resolved (Fig. 2).

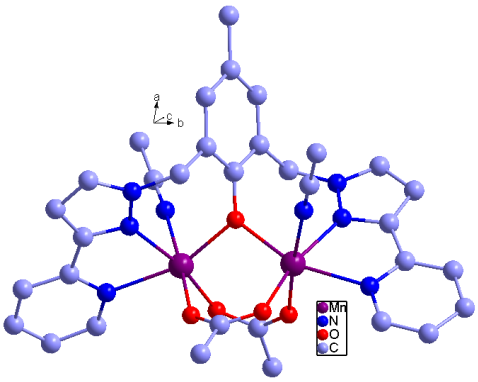

Fig. 1. View of the structure of $[Mn^{II}_2(\mu\text{-}OL^1)(\mu\text{-}OAc)_2(CH_3CN)_2]^+$. Hydrogen atoms are omitted for clarity.

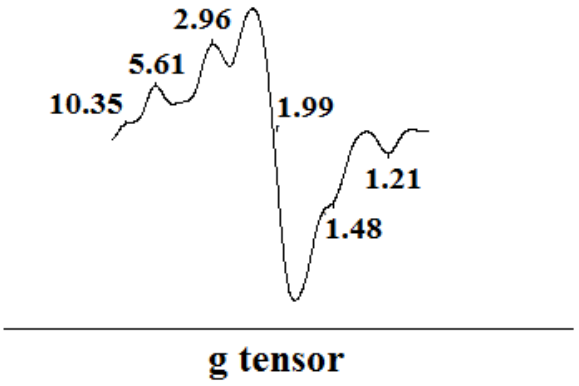

Fig. 2. Polycrystalline X-band EPR spectrum of (**1b**) at 120 K

Redox Properties. Cyclic voltammetric experiment was performed on **1a** in CH_3CN (TBAP as supporting electrolyte) at a platinum working electrode (Fig. 3). A quasi-reversible

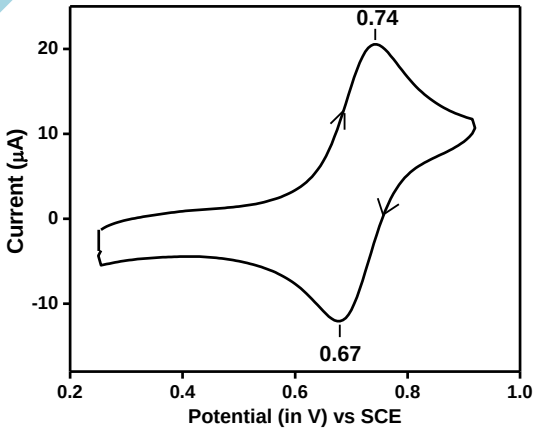

Fig. 3. Cyclic voltammogram (100 mV/s) of a ~1.0 mM solution of (**1a**) at a platinum electrode in CH_3CN (0.1 M in TBAP). Indicated potentials (in V) are vs SCE.

redox process with $E_{1/2}$ = 0.70 V vs SCE and ΔE_p = 70 mV, assigned to $[Mn^{III}Mn^{II}(\mu\text{-}OL)(\mu\text{-}OAc)_2(CH_3CN)_2]^{2+}/[Mn^{II}_2(\mu\text{-}OL)(\mu\text{-}OAc)_2(CH_3CN)_2]^+$ is observed. The high $E_{1/2}$ value indicates that the manganese(II) state is reasonably stabilized. This value lies in between those of other μ-phenoxo-bis(μ-carboxylato)dimanganese(II) complexes of acyclic dinucleating ligands.[18]

Nature of the one-electron oxidized species. Controlled-potential electrolysis of **1a** [0.015 g (1.71 x 10^{-5} mol)] in 15 mL of dry CH_3CN solution (0.1 M TBAP) consumed 1.62 x 10^{-5} F of charge, indicating a one-electron oxidation of the Mn^{II}_2 state to the $Mn^{III}Mn^{II}$ state. Due to oxidation the color changes from light yellow to purplish brown. On standing (~1h), the coulometrically oxidized solutions gradually faded to light yellow, indicating that $Mn^{III}Mn^{II}$ state is unstable. It is worth mentioning here that the Mn coordination sphere is provided by chelating arms of the ligand forming one five-membered and one seven-membered chelate ring. Seven-membered chelate ring is too large for the small Mn^{3+} ion (0.79 Å) thus destabilizing the Mn^{3+} ion with respect to reduction back to Mn^{2+} ion (0.99 Å).

The purplish-brown solution obtained due to coulometric oxidation of **1a** (see below) shows absorption peak at 510 nm (900 M^{-1} cm^{-1}), which is tentatively assigned due to phenolate-to-Mn^{III} charge-transfer transition (Fig. 4(a)). For $Mn^{III}Mn^{II}$ state, if they are antiferromagnetically coupled, they will have an S = 1/2 ground state, which gives a characteristic EPR spectrum centered at g = 2. Mixed-valence state can exhibit

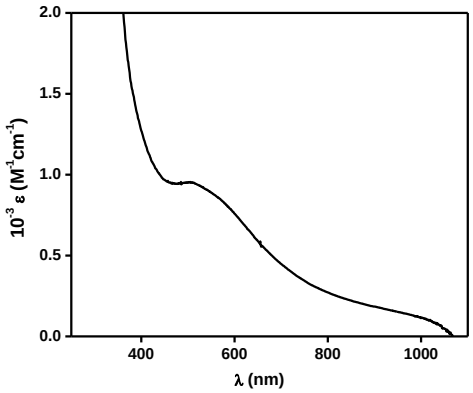

Fig. 4. (a) Absorption spectrum of coulometrically-generated one-electron oxidized species of **1a** (**1a**$^+$).

between 16 and 36 hyperfine lines. In our system, it gives six weak hyperfine-splitting centered at g = 2 (Fig. 4(b)). So, from EPR spectral result it is not possible to say whether the mixed-valence state is localized ($Mn^{III}Mn^{II}$) or delocalized ($Mn^{2.5}Mn^{2.5}$). Most probably, this is a $Mn^{III}Mn^{II}$ state, given the lack of literature report till date where $Mn^{2.5}Mn^{2.5}$ state is reported.[19] We do not expect completely delocalized $Mn^{2.5}Mn^{2.5}$ state in phenolate-bridging ligand system.

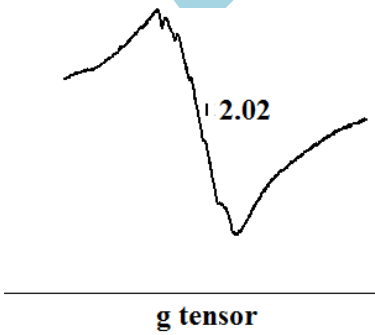

Fig. 4. (b) X-band EPR spectrum (CH3CN; 120 K) of (1a$^+$).

Computational Results. In order to ascertain the nature of the redox-active orbitals involved in the oxidation of complex **1b**, DFT calculations were performed on the parent complex **1b** as well as on its one-electron oxidized species **1b(ox)**. The results are presented in Tables 1 and 2.

Natural population analysis (NPA) and Gross electron population analysis were done on **1b** and **1b(ox)** to investigate which one of the two manganese ions is loosing the electron during oxidation of **1b** to **1b(ox)**. It is observed that when complex **1b** is oxidized to **1b(ox)** in both complexes Mn-ligand bond distances do not change for Mn1 (comparison of bond lengths). On the other hand, for Mn2, a significant decrease in Mn-ligand bond distances is observed. While oxidation of the complex **1b**, as Mn2 looses electron, the ligand donates more electron density to the metal and thus Mn-ligand bond lengths are decreased, and bond orders are increased. Natural population analysis shows that the charge and spin density of Mn1 atom remains same for both, **1b** as well as **1b(ox)**, while Mn2 shows an increase of 0.37 in atomic charge and a decrease of 0.78 in spin density when complex **1b** is oxidized to **1b(ox)**.

Table 1a. Mn1-Ligand bond distances, NPA-derived Mn1 atomic charges (q_{NPA}) and spin densities (SD_{NPA}) in the **1b** and **1b(ox)** complexes.

Complexes	Bond Lengths					q_{NPA} (a.u.)	SD_{NPA} (a.u.)
	Mn-N_{py}	Mn-N_{pyz}	Mn-OAc	Mn-OAc	Mn-O_{phenol}		
1b	2.235	2.192	2.072	2.075	2.124	1.56	4.82
1b(ox)	2.195	2.155	2.046	2.166	2.154	1.60	4.78

Table 1b. Mn2-Ligand bond distances, NPA-derived Mn2 atomic charges (qNPA) and spin densities (SDNPA) in the **1b** and **1b(ox)** complexes.

Complexes	Bond Lengths					q_{NPA} (a.u.)	SD_{NPA} (a.u.)
	Mn-N_{py}	Mn-N_{pyz}	Mn-OAc	Mn-OAc	Mn-O_{phenol}		
1b	2.242	2.187	2.081	2.064	2.117	1.55	4.82
1b(ox)	2.084	2.003	2.053	1.890	1.922	1.92	4.04

Gross electron population analysis on **1b** and **1b(ox)** further helps to ensure that electron is lost by only one of the MnII ion. Number of total electrons on Mn1 is constant (23.36) in complex **1b** as well as complex **1b(ox)**. At the same time, number of electrons on Mn2 changes from 23.36 in complex **1b** to 23.02 in complex **1b(ox)**. It is also clear from the HOMO pictures of **1b** and **1b(ox)**. In **1b** both MnII ions have almost same electron density (Fig. 5a) while in complex **1b(ox)** the electron density is localized on one of the Mn ions. (Fig. 5b).

Table 2a. Gross electron population on Mn1 and ligand fragments of **1b** and **1b(ox)** complexes.

Gross Electron Population	**1b**			**1b(ox)**		
	Mn s,p	Mn d	Ligand	Mn s,p	Mn d	Ligand
Alpha spin	9.00	5.08	164.74	9.00	5.05	164.46
beta spin	9.00	0.28	164.37	9.00	0.28	164.15
Alpha-beta	0	4.8	0.37	0	4.77	0.31
Total	18.00	5.36	329.11	18.00	5.33	328.61

Table 2b. Gross electron population on Mn2 and ligand fragments of **1b** and **1b(ox)** complexes.

Gross Electron Population	**1b**			**1b(ox)**		
	Mn s,p	Mn d	Ligand	Mn s,p	Mn d	Ligand
Alpha spin	9.00	5.08	164.74	9.00	4.51	164.46
beta spin	9.00	0.28	164.37	9.00	0.51	164.15
Alpha-beta	0	4.8	0.37	0	4.00	0.31
Total	18.00	5.36	329.11	18.00	5.02	328.61

Both the α-spin HOMO (Fig. 5b) and LUMO of **1b(ox)** are bonding orbitals. These two molecular orbitals (MOs) have 70% and 62% metal orbital contributions (Table 3).

Table 3. α-Spin frontier molecular orbitals of **1b(ox)** obtained from DFT calculations

Molecular Orbital	Energy eV	Symmetry	Orbital Contributions from Fragments %		
			Mn1	Mn2	Ligand
LUMO+5	–5.23	A	0	0	100
LUMO+4	–5.3	A	1	0	99
LUMO+3	–5.87	A	0	1	99
LUMO+2	–6.11	A	3	0	97
LUMO+1	–6.77	A	0	2	98
LUMO	–7.48	A	4	58	39
HOMO	–9.03	A	65	5	30
HOMO-1	–9.69	A	70	1	28
HOMO-2	–10.71	A	55	10	35
HOMO-3	–10.76	A	65	5	30
HOMO-4	–10.93	A	79	4	17
HOMO-5	–10.97	A	50	12	38

If the metal-ligand bonding in the complex were only ionic with no covalent contributions, these two MOs would be 100% metal-based. The 1e- reduction will lead to addition of electron to the α-spin LUMO as α-spin LUMO (–7.48 eV) is at lower energy than β-spin LUMO (–7.01 eV). Because of the bonding nature of these two orbitals, it can be expected that reduction of the **1b(ox)** species can lead to significant changes in metal-ligand bonding and these redox processes involve both the metal atoms and the phenolate ligand. This is corroborated by the electron population analysis of molecular fragments in **1b** and **1b(ox)** (Table 2). In going from **1b** to **1b(ox)**, the MPA-derived electron populations of the Mn1 atom are 23.36 and 23.33 electrons, respectively (Table 2a), while for the pure ionic bonding situation, the electron population of the Mn1 atom would be 23 electrons in both complexes (if Mn1 center does not get affected by the redox process). Similarly for the Mn2 atom, in going from **1b** to **1b(ox)**, the MPA-derived electron populations change from 23.36 electrons to 23.02 electrons, respectively (Table 2b), while for the pure ionic bonding satiation, the electron populations of the Mn2 atom would be 23 and 22 electrons, respectively. Thus, these electron population results indicate that **1b** and **1b(ox)** are

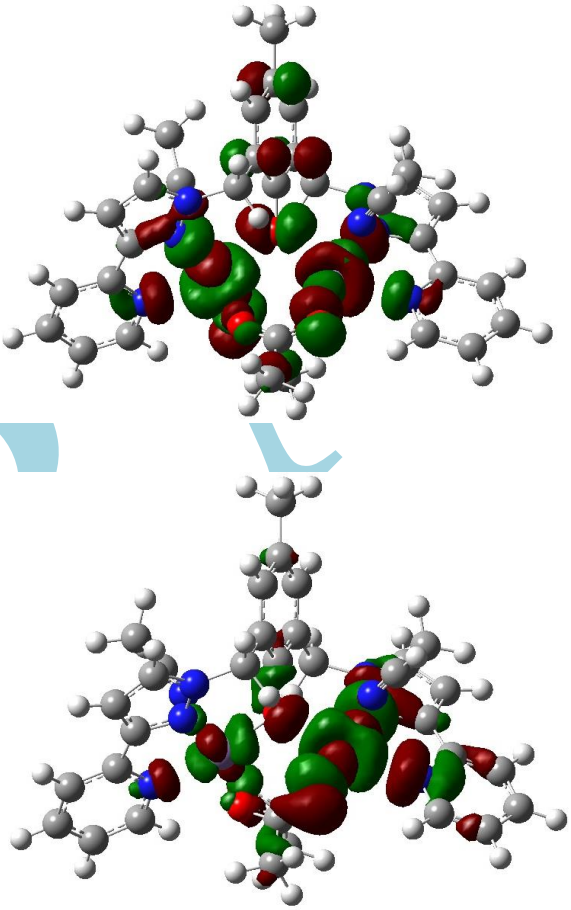

Fig. 5 α-spin (a) HOMO for **1b** (above) and (b) HOMO for the **1b(ox)** (below) cation (orbital contour values are 0.02).

covalently-coupled metal-ligand systems and the degree of the metal-ligand covalency strongly depends upon the oxidation state of the metal ion. Increase of the oxidation state of the central atom opens up metal 3d-based acceptor orbitals (dx^2-y^2, dz^2) and brings these closer to the ligand donor orbitals. This results in higher ligand-to-metal donation (0.36 for **1b**, 0.33 for **1b(ox)** ligand to Mn1 atom and 0.36 for **1b** and 1.02 for **1b(ox)** ligand to Mn2 atom) and, thus, higher metal-ligand covalency which in turn reduces the higher metal atomic charge on the metal ion. Such strong electronic coupling between the central metal ion and the phenolate ligand implies that the phenolate ligand is redox non-innocent and the properties of the corresponding species will strongly depend to the metal-ligand covalency. Based on the analysis of the wave functions of the complexes (Tables 1 and 2), the **1b(ox)** complex with the d^4, d^5 configuration has more covalent Mn-ligand bonds than the 1b complex with the high-spin d^5 configuration.

IV. Summary and Conclusions

In this work, redox property of complex **1a** has been investigated. Cyclic voltammetric experiments show a quasireversible process at $E_{1/2}$ = 0.70 V vs SCE. Coulometric

oxidation in dry CH_3CN produced the one-electron oxidation product $Mn^{III}Mn^{II}$, which is found to be unstable towards reduction. We assign the electronic structure of $Mn^{II}Mn^{II}$ dimer and its one-electron oxidized product $Mn^{III}Mn^{II}$ through DFT calculations. During one-electron oxidation of **1b** only one Mn atom is losing electron and other one is redox innocent. DFT calculations indicate that the redox process has significant ligand character. Increase in the oxidation state of Mn^{II} results in enhanced charge donation from ligand to metal ion. Increased metal-ligand covalency in turn compensates for the higher positive charge on the metal ion. Such strong electronic coupling between the metal ion and the phenolate ligand implies that the phenolate ligands are redox non-innocent and the properties of the corresponding species will strongly depend to the metal-ligand covalency.

Acknowledgment

H.A. gratefully acknowledges the award of an SRF by the Council of Scientific & Industrial Research, Government of India. H.A. acknowledges Prof. R. N. Mukherjee whose guidance helped me in shaping this result.

References

[1] (a) B. P. Murch, P. Boyle, L. Que, Jr. Structures of binuclear and tetranuclear iron(III) complexes as models for ferritin core formation. J. Am. Chem. Soc. 1985, 107, 6728-6729. (b) B. P. Murch, F. C. Bradley, L. Que, Jr. A binuclear iron peroxide complex capable of olefin epoxidation. J. Am. Chem. Soc. 1986, 108, 5027-5028. (c) A. S. Borovik, B. P. Murch, L. Que, V. Papaefthymiou, E. Munck, Jr. Models for iron-oxo proteins: a mixed valence iron (II)-iron (III) complex. J. Am. Chem. Soc. 1987, 109, 7190-7191. (d) Q. Chen, J. B. Lynch, P. Gomez-Romero, A. Ben-Hussein, G. Jameson, C. J. O'Connor, L. Que, Jr. Iron-oxo aggregates. Binuclear and tetranuclear complexes of N,N,N',N'-tetrakis(2-benzimidazolylmethyl)-2-hydroxy-1,3-diamino propane. Inorg. Chem. 1988, 27, 2673-2681.

[2] (a) A. S. Borovik, L. Que, Jr. Models for the iron(II)iron(III) and iron(II)iron(II) forms of iron-oxo proteins J. Am. Chem. Soc. 1988, 110, 2345-2347. (b) A. S. Borovik, V. Papaefthymiou, L. F. Taylor, O. P. Anderson, L. Que, Jr. Models for iron-oxo proteins. Structures and properties of $Fe^{II}Fe^{III}$, $Zn^{II}Fe^{III}$, and $Fe^{II}Ga^{III}$ complexes with (μ-phenoxo)bis(μ-carboxylato)dimetal cores. J. Am. Chem. Soc. 1989, 111, 6183-6195. (c) A. S. Borovik, M. P. Hendrich, T. R. Holman, E. Münck, V. Papaefthymiou, L. Que, Jr. Models for diferrous forms of iron-oxo proteins. Structure and properties of $[Fe_2BPMP(O_2CR)_2]BPh_4$ complexes. J. Am. Chem. Soc. 1990, 112, 6031-6038.

[3] (a) M. S. Mashuta, R. J. Webb, J. F. McCusker, E. A. Schmitt, K. J. Oberhausen, J. F. Richardson, R. M. Buchanan, D. N. Hendrickson, Electron transfer in iron(II)iron(III) model complexes of iron-oxo proteins. J. Am. Chem. Soc. 1992, 114, 3815-3827. (b) M. S. Mashuta, R. J. Webb, K. J. Oberhausen, J. F. Richardson, R. M. Buchanan, D. N. Hendrickson, Valence detrapping in iron(II)-iron(III) models of iron-oxo proteins. J. Am. Chem. Soc. 1989, 111, 2745-2746.

[4] (a) J. R. Hartman, R. L. Rardin, P. Chaudhuri, K. Pohl, K. Wieghardt, B. Nuber, J. Weiss, G. C. Papaefthymiou, R. B. Frankel, S. J. Lippard, Synthesis and characterization of (μ-hydroxo)bis(μ-acetato)diiron(II) and (μ-oxo)bis(μ-acetato)diiron(III) 1,4,7-trimethyl-1,4,7-triazacyclononane complexes as models for binuclear iron centers in biology; properties of the mixed valence diiron(II,III) species. J. Am. Chem. Soc. 1987, 109, 7387-7396. (b) K. S. Murray, The Magnetochemistry of Homo-and Hetero-Tetranuclear First-Row d-Block Complexes. Coord. Chem. Rev. 1974, 12, 1-15.

[5] (a) R. S. Reczkowski, D. E. Ashe, EPR evidence for binuclear manganese(II) centers in rat liver arginase J. Am. Chem. Soc. 1992, 114, 10992-10994. (b) S. V. Khangalov, P. J. Pessiki, V. V. Baryinin, D. E. Ashe, G. C. Dismukes, Determination of the Metal Ion Separation and Energies of the Three Lowest Electronic States of Dimanganese(II,II) Complexes and Enzymes: Catalase and Liver Arginase. Biochemistry, 1995, 34, 2015-2025. (c) G. C. Dismukes, Manganese Enzymes with Binuclear Active Sites. Chem. Rev. 1996, 96, 2909-2926. (d) M. J. Jedrzejas, M. Chander, P. Setlow, G. Krishnasamy, Mechanism of catalysis of the cofactor-independent phosphoglycerate mutase from bacillus stearothermophilus, crystal structure of the complex with 2-phosphoglycerate. J. Biol. Chem. 2000, 275, 23146-23156. (e) J. N. Beal, P. J. O'Malley, Manganese Oxidation State Assignment for Manganese Catalase. J. Am. Chem. Soc. 2016, 138 (13), 4358-4361.

[6] M. J. Jedrzejas, P. Setlow, Comparison of the Binuclear Metalloenzymes Diphosphoglycerate-Independent Phosphoglycerate Mutase and Alkaline Phosphatase: Their Mechanism of Catalysis via a Phosphoserine Intermediate. Chem. Rev. 2001, 101, 607-618.

[7] (a) K. D. Karlin, R. W. Cruse, Y. Gultneh, J. C. Hayes, J. A. Zubieta, Peroxide coordination to a dicopper(II) center. Dioxygen binding to a structurally characterized phenoxide-bridged binuclear copper(I) complex. J. Am. Chem. Soc. 1984, 106, 3372-3374. (b) P. J. Pessiki, G. C. Dismukes, Structural and functional models of the dimanganese catalase enzymes. 3. Kinetics and mechanism of hydrogen peroxide dismutation. J. Am. Chem. Soc. 1994, 116, 898-903.

[8] Y. Gultneh, B. Ahvazi, A. R. Khan, R. J. Butcher, J.-P. Tuchagues, Modeling the Multinuclear Redox-Active Manganese Enzymes. Synthesis, Structure, and Properties of a Bis(dinuclear Mn(III)-.mu.-oxo-bis(.mu.-acetato)) Complex. Inorg. Chem. 1995, 34, 3633-3645.

[9] H. Chermette, Density functional theory: A powerful tool for theoretical studies in coordination chemistry. Coord. Chem. Rev. 1998, 699, 178-180.

[10] H. Arora, S. K. Barman, F. Lloret, R. N. Mukherjee, Isostructural Dinuclear Phenoxo-/Acetato-Bridged Manganese(II), Cobalt(II), and Zinc(II) Complexes with Labile Sites: Kinetics of Transesterification of 2-Hydroxypropyl-p-nitrophenylphosphate. Inorg. Chem. 2012, 51, 5539-5553.

[11] A. J. Amoroso, A. M. C. Thompson, J. C. Jeffery, P. L. Jones, J. A. McCleverty, M. D. Ward, Synthesis of the new tripodal ligand tris-[3-(2′-pyridyl)pyrazol-1-yl]hydroborate, and the crystal structure of its europium(III) complex. J. Chem. Soc. Chem. Commun. 1994, 2751-2752.

[12] (a) M. Ray, S. Mukerjee, R. Mukherjee, Manganese(III) Complexes of 1,2-Bis(2-pyridinecarboxamido)benzene: Synthesis, Spectra and Electrochemistry. J. Chem. Soc., Dalton Trans. 1990, 3635-3638. (b) N. Gupta, S. Mukerjee, S. Mahapatra, M. Ray, R. Mukherjee, Triply bridged diruthenium complexes with $[Ru^{III}_2(\mu\text{-}O)(\mu\text{-}O_2CCH_3)_2]^{2+}$ and $[Ru^{IV}Ru^{III}(\mu\text{-}O)(\mu\text{-}O_2CCH_3)_2]^{3+}$ cores: synthesis, spectra, and electrochemistry. Inorg. Chem. 1992, 31, 139-141.

[13] M. J. Frisch, G. W. Trucks, H. B. Schlegel, G. E. Scuseria, M. A. Robb, J. R. Cheeseman, J. A. Montgomery, T. Vreven, K. N. Kudin, J. C. Burant, J. M. Millam, S. S. Lyengar, J. Tomasi, V. Barone, B. Mennucci, M. Cossi, G. Scalmani, N. Rega, G. A. Petersson, H. Nakatsuji, M. Hada, M. Ehara, K. Toyota, R. Fukuda, J. Hasegawa, M. Ishida, T. Nakajima, Y. Honda, O. Kitao, H. Nakai, M. Klene, X. Li, J. E. Knox, H. P. Hratchian, J. B. Cross, C. Adamo, J. Jaramillo, R. Gomperts, R. E. Stratmann, O. Yazyev, A. J. Austin, R. Cammi, C. Pomelli, J. W. Ochterski, P. Y. Ayala, K. Morokuma, G. A. Voth, P. Salvador, J. J. Dannenberg, V. G. Zakrzewski, S. Dapprich, A. D. Daniels, M. C. Strain, O. Farkas, D. K. Malick, A. D. Rabuck, K. Raghavachari, J. B. Foresman, J. V. Ortiz, Q. Cui, A. G. Baboul, S. Clifford, J. Cioslowski, B. B. Stefanov, G. Liu, A. Liashenko, P. Piskorz, I. Komaromi, R. L. Martin, D. J. Fox, T. Keith, M. A. Al-Laham, C. Y. Peng, A. Nanayakkara, M. Challacombe, P. M. W. Gill, B. Johnson, W. Chen, M. W. Wong, C. Gonzalez, J. A. Pople, Gaussian 03 Revision C.01.

[14] A. D. Becke, Density-functional thermochemistry. III. The role of exact exchange. J. Chem. Phys. 1993, 98, 5648.

[15] R. S. Mulliken, Electronic Population Analysis on LCAO–MO Molecular Wave Functions. J. Chem. Phys. 1955, 23, 1833.

[16] A. E. Reed, R. B. Weinstock, F. Weinhold, Natural population analysis. J. Chem. Phys. 1985, 83, 735.

[17] (a) S. V. Khangulov, V. V. Barynin, N. V. Voevodskaya, A. I. Grebenko, ESR spectroscopy of the binuclear cluster of manganese ions in the active center of Mn-catalase from Thermus thermophilus. Biochim. Biophys. Acta 1990, 1020, 305-310. (b) P. J. Pessiki, S. V. Khangulov, D. M. Ho, G. C. Dismukes, Structural and Functional Models of the Dimanganese Catalase Enzymes. Structure, Electrochemical, Redox, and EPR Properties. J. Am. Chem. Soc. 1994, 116, 891-897. (c) I. Romero, L. Dubois, M.-N. Collomb, A. Deronzier, J.-M. Latour, J. Pecaut, A Dinuclear Manganese(II) Complex with the $\{Mn_2(\mu\text{-}O_2CCH_3)_3\}^+$ Core: Synthesis, Structure, Characterization, Electroinduced Transformation, and Catalase-like Activity. Inorg. Chem. 2002, 41, 1795-1806.

[18] C. Higuchi, H. Sakiyama, H. Okawa, D. E. Fenton, Dimanganese(II) complexes of a new phenol-based dinucleating ligand with two amino chelating arms: synthesis, structure and catalase-like activity. J. Chem. Soc., Dalton Trans. 1995, 4015-4020.

[19] (a) H. Sakiyama, A. Sugawara, M. Sakamoto, K. Unoura, K. Inoue, M. Yamasaki, Manganese(II) complexes of an acyclic phenol-based dinucleating ligand with four methoxyethyl chelating arms: synthesis, structure, magnetism and electrochemistry. Inorg. Chim. Acta 2000, 310, 163-168. (b) Y. Gultneh, Y. T. Tesema, T. B. Yisgedu, R. J. Butcher, G. Wang, G. T. Yee, Studies of a Dinuclear Manganese Complex with Phenoxo and Bis-acetato Bridging in the Mn_2(II,II) and Mn_2(II,III) States: Coordination Structural Shifts and Oxidation State Control in Bridged Dinuclear Complexes. Inorg. Chem. 2006, 45, 3023-3033. (c) Y. Gultneh, Y. T. Tesema, B. Ahvazi, T. B. Yisgedu, R. J. Butcher, J.-P. Tuchagues, Structure and characterization of a μ-phenoxo-bis μ-acetato dinuclear Mn(II,II) complex $[Mn_2(LO)(\mu\text{-}OAc)_2](ClO_4)$ (LOH = 2,6-bis{bis(2-(2-pyridyl)ethyl)aminomethyl}-4-methylphenol): Substituent effects Inorg. Chim. Acta 2006, 359, 4463-4469.

